

Time-resolved four-wave-mixing spectroscopy of excitons in a single quantum well

J. A. Davis,¹ J. J. Wathen,¹ V. Blanchet,^{1,2} and R. T. Phillips¹

¹*Cavendish Laboratory, University of Cambridge, J.J. Thomson Avenue, Cambridge CB3 0HE, United Kingdom*

²*Laboratoire Collisions Agrégats Réactivité-IRSAMC-CNRS-Université Paul Sabatier, Toulouse, France*

(Received 13 April 2006; published 11 January 2007)

We have investigated, by fully-time-resolved degenerate four-wave mixing (FWM), excitonic coherence phenomena in single GaAs/AlGaAs quantum wells which are known to exhibit localization. A magnetic field (0–12 T) was applied in Faraday geometry as a means of altering the nature of the excitonic transitions in a controlled manner. When the system is excited by a sequence of pulses tuned in resonance with the heavy-hole excitons, the predominant behavior observed at positive interpulse delays is beating in the FWM emission due to polarization interference between uncoupled excitons localized by monolayer islands. For negative interpulse delay the variation of beat phase with delay changes sign as the magnetic field is increased. In order to understand this feature, we modeled a coupled three-level system and included local field effects as a simple phenomenological approach to describing many-body terms. Comparison with experiments shows that with a larger magnetic field, the contribution to the signal from the coupled system reduces while that from two noninteracting two-level systems increases. We attribute this to the increased confinement of the excitons with field, leading to reduced wavefunction overlap, and hence reduced coupling.

DOI: [10.1103/PhysRevB.75.035317](https://doi.org/10.1103/PhysRevB.75.035317)

PACS number(s): 78.30.Ly, 71.23.-k, 71.35.Cc

I. INTRODUCTION

Heterodyne detection of four-wave mixing (FWM) has allowed significant gain in sensitivity due to its dependence on electric field amplitude rather than intensity.^{1–4} The technique is essentially interferometric, and since the signal is obtained by mixing the four-wave-mixing output with part of the original pulse, the method has the added advantage of being intrinsically time-resolved. This improved sensitivity and time resolution has opened the prospect of revisiting various phenomena which have not previously been fully explained. One such unresolved problem concerns the origin and nature of the beats observed between different monolayer islands in a single quantum well.

Time-resolved FWM (TR-FWM) experiments on GaAs/AlGaAs quantum wells performed in 1993 by Koch *et al.*⁵ showed that the third-order polarization of the sample produces a photon-echo-like signal, modulated both in its real-time profile and as a function of delay, τ , between the exciting pulses. These oscillations arise from simultaneous excitation of excitons localized by different monolayer islands of the quantum well and were assigned to quantum beating, indicating that different islands are coupled to each other. Previous work⁶ had shown that quantum beats (QB) and polarization interference (PI) (interferences at the detector between optical signals emitted from different and otherwise uncoupled two-level systems) can be distinguished in TR-FWM by observing the change in phase of the beats with interpulse delay τ . τ corresponds to the interval between pulse 1, arriving with wave vector k_1 , and pulse 2, with wave vector k_2 . τ is positive when we are considering the FWM signal emitted in the $2k_2 - k_1$ direction, and pulse 1 arrives before pulse 2. The FWM signal is resolved as a function of t , the real time of evolution, where $t=0$ corresponds to the arrival of pulse 2 at the sample. The phase of the QB in t varies with the arrival of pulse 2 while that of PI varies with interpulse delay in the same manner as a photon echo (PE).

This approach provided in the work of Koch *et al.*⁵ a clear, yet surprising, indication that different monolayer islands were coupled in some way and could not be represented by two independent two-level systems.

This picture was, however, challenged by Euteneuer *et al.*⁷ who performed coherent excitation spectroscopy on samples similar to those used by Koch *et al.*, and they concluded that there was no coherent coupling between different monolayer islands. Finger *et al.*⁸ suggested that the explanation for this apparent contradiction is that the beats observed in the earlier work did not arise from monolayer fluctuations, but from biexcitons beating with excitons.⁹ There have been other attempts to clarify the nature of the coupling, or lack thereof, between different monolayer islands,^{10–12} but no consensus has emerged.

Modeling of the beating between light- and heavy-hole excitons by Smirl *et al.*¹³ showed that within the phenomenological few-level approximation, the introduction of terms describing excitation-induced dephasing¹⁴ (EID) gives good qualitative agreement with experiment. EID is one means of introducing behavior into the phenomenological model which mimics some features expected in an underlying microscopic description in terms of the many-body response. Furthermore, in their work, Smirl *et al.* showed clear experimental evidence of many-body correlations beyond those of the semiconductor Bloch equations. Kwong *et al.*¹⁵ have explored the relationship between the terms in the few-level models and the microscopic formulation, and have shown that it is possible to make a conversion between the parameters deduced from the few-level approach and those of the more fundamental treatment, including those describing EID and local fields. Clearly there is scope for further investigation of both the nature of the coupling in the system based on excitons localized in islands, and of the fitting with phenomenological models.

We hope to shed some light on the nature of the coupling by using heterodyne detection to perform TR-FWM experiments on a single 10.0 nm GaAs quantum well with AlGaAs

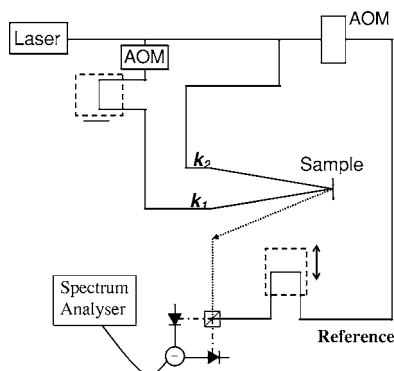


FIG. 1. A schematic diagram of the arrangement of the four-wave-mixing interaction and the heterodyne detection scheme.

barriers. The growth was interrupted to allow monolayer islands to form, resulting in a sample similar to those studied earlier. To explore further the nature of the states and the effects of localization, we applied a magnetic field perpendicular to the well, which should confine the exciton to a progressively smaller area in the plane of the quantum well as the field is increased.¹⁶ The experimental details and results are discussed in Sec. II.

In order to explain the unexpected and interesting effects observed at negative τ , we have simulated both a coupled three-level system and two noninteracting two-level systems, by simple optical Bloch equations. As an alternative to inclusion of EID as a means of introducing phenomenologically the many-body effects, we have chosen to include local fields in the calculations;^{17,18} the most important effect of this is to allow a qualitative approach to modeling the signal at negative delays. The model is presented in Sec. III and the results of the simulations discussed and compared to the experimental results in Sec. IV. A summary and conclusion are given in Sec. V.

II. EXPERIMENT AND RESULTS

A mode-locked titanium:sapphire laser is used as a source of pulses of duration 200 fs. The laser output is split into three beams labeled k_1 , k_2 , and ‘reference’ in the schematic diagram of the experiment in Fig. 1. Beam 1 passes through an acousto-optic modulator (AOM) resulting in a shift of all the optical frequencies by $-\omega_{k_1}$, the modulation frequency of the AOM. The FWM is detected in the ‘reflection’ geometry,¹⁹ in order to avoid the need to thin the substrate; this signal has frequencies $\omega_0 + \omega_{k_1}$, where ω_0 is a frequency in the pulse spectrum of the unmodulated laser. The reference beam passes through another AOM, which modulates it at a slightly different frequency ω_R , leading to an increase in the optical frequency by this amount. The FWM signal and the reference beam are recombined via a cube beam splitter. The two outputs of the beam splitter are coupled to a pair of balanced photodiodes. The optical interferences detected by each photodiode are modulated at the difference frequency of the reference and signal beams, $|\omega_{k_1} - \omega_R|$. The amplitude of these beats is proportional to the electric field of the FWM signal, and is measured with about 6 decades of dynamic

range using a spectrum analyzer. The beams incident on the sample are cocircularly polarized in order to ensure that no biexcitons are created, and are of power such that the excitation density is approximately $4 \times 10^9 \text{ cm}^{-2}$. In order to maximize the optical interference used to resolve the time-profile of the signal, the polarization of the signal is made linear by a $\lambda/4$ waveplate before the cube beam splitter. The magnetic field is applied perpendicular to the plane of the well by a superconducting magnet capable of fields up to 12 T. The temperature of the sample is maintained at 5 K in order to minimize the effects of inhomogeneity. The results presented here correspond to the creation of σ^+ excitons, but the conclusions are similar for σ^- excitons. The sample was grown by molecular beam epitaxy (MBE) on an undoped [001] GaAs substrate and contains five GaAs wells of different widths ranging from 2.8 to 20.0 nm separated by 25.0 nm $\text{Al}_{0.37}\text{Ga}_{0.63}\text{As}$ barriers. At each interface the growth was interrupted for just over two minutes to allow monolayer islands to form. These islands are known to vary in size and shape and can be up to tens of nm in diameter, in the range of the exciton Bohr diameter.²⁰ For the purpose of this paper we will concentrate on the results from the 10.0 nm well only. This width corresponds to ≈ 35 monolayers of GaAs. Photoluminescence excitation spectroscopy shows that the 1s heavy-hole exciton transition is at ~ 1.552 eV with a doublet structure with a splitting ~ 1.6 meV. The 1s light-hole exciton transition lies 10 meV higher in energy. In the present experiment, contributions from the light-hole exciton are almost out of resonance and therefore not expected to be excited significantly. The TR-FWM results with magnetic field at 2, 4, and 10 T are shown in Figs. 2(a)–2(c). In these figures $\log_{10}(\text{DFWM amplitude})$ is plotted for each value of time interval between the input pulses (which can be read from the labels on the right). In each plot, the zero on the real-time axis is determined by the arrival of pulse 2, in contrast to the plots of Koch *et al.*,⁶ where the zero is determined by the arrival of pulse 1. The effect of this is that the phase of the beats is unchanged with τ for QB. For PI, it evolves in these plots in the same sense as for the photon echo, that is, with unit gradient. On this basis, it appears that in all cases the beats are mainly due to PI and not QB. However, closer examination shows that there is some modulation of the peak height of the beats with a period equal to the period of the real-time beats. This is represented in Fig. 3 for $B=11$ T. Here the TR-FWM has been integrated over the real-time of evolution t and its logarithm plotted as a function of the interpulse delay τ . This suggests there may also be some QB present.⁶ The traces around $\tau=0$ appear noisy; this is not in fact the case as most of the structure is reproducible, and caused by beating among the various coherently coupled levels of the system within the excitation envelope. The higher-frequency components correspond to large energy splittings of upper levels, which rapidly decohere after the excitation has passed. The character of the emission appears to undergo a transition from free polarization decay (FPD) to photon echo (PE) behavior. In all the data, it appears that at short interpulse delay FPD dominates before the bulk of the signal is transferred to the PE. It is possible that there are two separate components contributing to these two regimes.^{10,21} However, the most likely explanation is simply

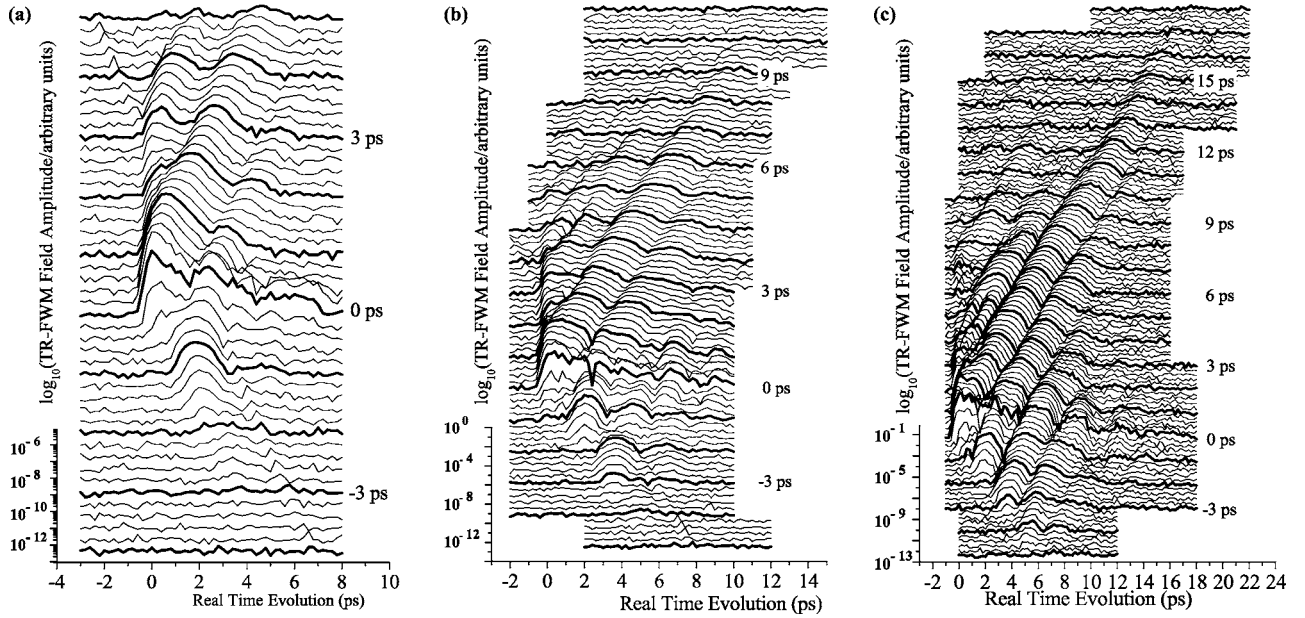


FIG. 2. (a) Time-resolved FWM signals at a field of 2 T. Each curve depicts the $\log_{10}(\text{FWM amplitude})$ (scale at the left), displaced uniformly according to the interpulse delay (labeled on the right-hand side). Details of the conditions are given in the text. (b) \log_{10} of the time-resolved FWM signals at a field of 4 T. (c) \log_{10} of the time-resolved FWM signals at a field of 10 T.

that the inhomogeneous broadening is relatively weak, and so at short delays, many of the excitons are still in phase, allowing FPD to dominate, and it is not until later that the majority have evolved to be out of phase and the PE dominates.^{21,22}

The effect of the magnetic field is most evident in the dephasing times. It is measured to be 3.0 ± 0.5 ps, 5 ± 1 ps, and 8 ± 1 ps for Figs. 2(a)–2(c), respectively. The effect of the field is to increase transverse exciton confinement, which reduces the exciton scattering cross-section and therefore increases the dephasing time.

It is also evident that as the magnetic field increases, the time for which FPD dominates increases, which suggests that the exciton population is increasingly homogeneous. This also is consistent with the reduction in size of the exciton wave function due to the magnetic field, as magnetic confinement progressively dominates over the inhomogeneity arising from the localization potential.¹⁰

The other effect of the magnetic field is observed in the signal at negative τ . At high fields, as shown in Fig. 2(c), the beats for $\tau < 0$ evolve with τ in the same sense as do the beats for $\tau > 0$, with gradient +1 with respect to τ . In Fig. 2(b), at intermediate fields, the phase of the beats at negative delay appears to be independent of τ , apart from a π phase change at one point. At 2 T, because the signal is so short lived, it is not clear how the phase varies with τ . The interpretation of this signal is not immediately clear. Previous studies of the phase of beats^{5,6,12} have concentrated on positive delays and have lacked sensitivity to study properly effects at negative delays. Theoretical studies modeling quantum beating in three-level systems^{11,12,23} have neglected local-field effects and excitation-induced dephasing (which phenomenologically model the signal at negative delays), and those including such effects^{16,17} have only done so for a two-level system. Hence, in the following section we present

the details of our calculations for a three-level system including local-field effects, in order to gain some further insight into the origin of the behavior we observe in the experiment.

III. MODELING

Here we calculate perturbatively the FWM signal from a three-level system, using the simple density matrix approach, and including local-field effects. Terms are included to third order in a manner similar to that used originally by Yajima and Taira²⁴ for a two-level system without the local field. Inclusion of the local field allows the first-order polarization induced by pulse 2 to contribute to the FWM signal provided $T_2 > \tau$. This is particularly relevant for negative interpulse delay. The system under consideration consists of a ground state (labeled 1) and two closely spaced excited states (labeled 2 and 3) corresponding to two different 1 s HH exciton transitions in two different islands of the quantum well distinct by one monolayer. We need to solve numerically

$$i\hbar\dot{\rho} = [H, \rho], \quad (1)$$

where ρ is the density matrix and H is the Hamiltonian:

$$H = H_0 + \mu[E + LP] \quad (2)$$

with the transition dipole μ

$$\mu = \begin{bmatrix} 0 & \mu_{12} & \mu_{13} \\ \mu_{12}^* & 0 & 0 \\ \mu_{13}^* & 0 & 0 \end{bmatrix}. \quad (3)$$

H_0 is the unperturbed Hamiltonian with the eigenenergies on the leading diagonal, E is the applied electric field, L is the Lorentz local-field factor, and P is the polarization $P = \text{Tr}(\mu\rho)$. Note that we have explicitly suppressed the lower-

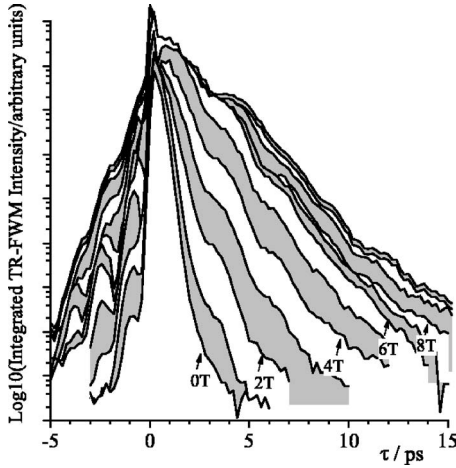


FIG. 3. Log_{10} (time-integrated FWM signal) in σ^+ polarization for magnetic fields from 0 T to 11 T in 1 T steps, as a function of the interpulse delay, τ . Note the modulation of the signals.

frequency transition between levels 2 and 3. Dephasing is included phenomenologically so that the diagonal components of the density matrix decay as $1/T_1$ and the off-diagonal components as $1/T_2$, corresponding to the longitudinal and transverse relaxation rates, respectively, with T_1 the lifetime of the relevant state and T_2 the coherence lifetime between the states, namely the ground state and the excited states $T_2(j)$ with $j=2,3$ or between the two excited states $T_2(ij)$. Note that these values may differ for the different levels and are not assumed to be the same. These are included as an extra term in the Hamiltonian such that:

$$\dot{\rho}_{jj}^{\text{Relax}} = -\frac{(\rho_{jj} - \rho_{jj}^0)}{T_{1(j)}} \quad (4)$$

and,

$$\dot{\rho}_{jk}^{\text{Relax}} = -\frac{\rho_{jk}}{T_{2(jk)}}, \quad (5)$$

where ρ_{jj}^0 is the equilibrium value for ρ_{jj} , with $j, k=1, 2, 3$ and $k \neq j$.

The local-field term is initially set to the Lorentz value, $1/(3\epsilon_0)$, as is generally used for cubic lattices. This term is really here to model the many-body effects that appear in a more complete treatment of the problem, and we will regard it as a parameter which can be used to improve the fit to the experimental results, rather than a given constant.

The excitation is described by two Gaussian pulses, 200 fs long, with frequency ω_0 , separated in time by τ , and with different wave vectors, k_1 and k_2 . In order to simplify the equations, the frame of reference is changed to one rotating at ω_0 , and the rotating-wave approximation is made, eliminating the terms varying rapidly at $\sim 2\omega_0$. This leads to changes in the Hamiltonian: $\omega_{j1} = \omega_{jj} - \omega_{11} - \omega_0$.

By multiplying out the matrices and expanding perturbatively to the third order, the following equations are obtained for the first three orders of the relevant density matrix elements:

$$\dot{\rho}_{1j}^{(1)} = \frac{-i}{\hbar} \mu_{1,j}^* [E + LP^{(1)}] - \rho_{1j}^{(1)} \left(\frac{1}{T_{2(j)}} - i(\omega_{j1}) \right) \quad (6)$$

$$\begin{aligned} \dot{\rho}_{jj}^{(2)} &= \frac{i}{\hbar} [\mu_{1j} \rho_{1j}^{(1)}] [E^* + LP^{(1)*}] \\ &\quad - \frac{i}{\hbar} [\mu_{1j}^* \rho_{1j}^{(1)*}] [E + LP^{(1)}] - \frac{1}{T_{1(j)}} (\rho_{jj}^{(2)}) \end{aligned} \quad (7)$$

$$\begin{aligned} \dot{\rho}_{23}^{(2)} &= \frac{i}{\hbar} \{ \mu_{12} \rho_{13}^{(1)} [E^* + LP^{(1)*}] - \mu_{13}^* \rho_{12}^{(1)*} [E + LP^{(1)}] \} \\ &\quad - \rho_{23}^{(2)} \left(\frac{1}{T_{2(23)}} - i\omega_{32} \right) \end{aligned} \quad (8)$$

$$\begin{aligned} \dot{\rho}_{1j}^{(3)} &= \frac{i}{\hbar} [E + LP^{(1)}] [\mu_{1j}^* (2\rho_{jj}^{(2)} + \rho_{kk}^{(2)}) + \mu_{1,k}^* \rho_{j,k}^{(2)*}] \\ &\quad - \frac{i}{\hbar} LP^{(3)} \mu_{1j}^* \\ &\quad - \rho_{1j}^{(3)} \left(\frac{1}{T_{2(j)}} - i\omega_{j1} \right), \end{aligned} \quad (9)$$

where $j=2, 3$, $k=2, 3 \neq j$, $T_{2(23)}$ is the coherence lifetime between the two excited states, and the frequencies are defined as $\omega_{j1} = \omega_j - \omega_1$ and $\omega_{32} = \omega_3 - \omega_2$. It is assumed that both μ and ρ are Hermitian, so $\mu_{kj} = \mu_{jk}^*$ and $\rho_{kj} = \rho_{jk}^*$, and all other terms not included are zero. The assumptions have been made that $\rho_{11} = 1 - \rho_{22} - \rho_{33}$, and the initial values of all terms are zero except $\rho_{11}^0 = 1$.

Rather than fully integrating these equations, the wave vector components of the electric field are identified, and only the terms which contribute to the third-order polarizations in the $2k_2 - k_1$ direction are kept. This creates a set of interdependent first-order linear differential equations which are given for reference in the Appendix. These equations are solved simultaneously using standard numerical methods, and values found for third-order terms in ρ_{12} and ρ_{13} with wave vector $2k_2 - k_1$. Inhomogeneous broadening is also taken into account by integrating over the inhomogeneous distribution. It is assumed that for the monolayer islands, the broadening is Gaussian and totally correlated.^{11,23,25} This assumption is based on minimal inhomogeneous broadening, so any effects due to uncorrelated broadening should be small.¹¹

IV. RESULTS OF THE SIMULATION

The simulation was run for a wide range of all the variable parameters: the results shown in Fig. 4 are for parameters similar to those determined from the experimental data in Fig. 2(b). The lifetimes and coherent lifetimes were assumed to be the same for both transitions, with $T_1 = 50$ ps and $T_2 = 4$ ps. The transition energies were set to be 1.5512 and 1.5528 eV, corresponding to the observed 1.6 meV beating. For simplification, the laser excitation lies in the middle of the two at 1.552 eV. The pulse length was chosen to be

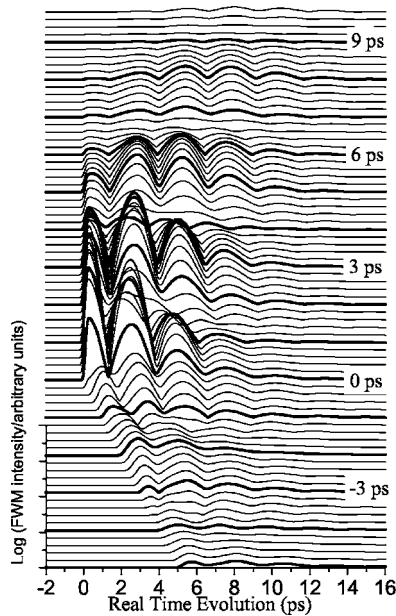


FIG. 4. Simulated log (TR-FWM) from a coupled three-level system with equal dipole matrix elements for the two transitions. Parameters are specified in the text.

200 fs, and the local-field term $\frac{1}{3\epsilon_0}$. The inhomogeneous broadening was set to 0.4 meV on the basis of the relative contributions displaying PE and FPD behavior. The plot in Fig. 4 shows the expected beats and predominant absence of any variation of their phase with τ . This is as expected from previous experiments⁵ and reproduces the TR-FWM signal from a three-level system calculated analytically by Zhu *et al.*¹¹ The calculated signal at negative delay indicates that the beats continue to evolve with no dependence on τ .

At the minima in the beats as a function of τ , the calculation shows beats almost π out of phase with the rest of the signal; this is a result of one small term whose phase varies in the same manner as a photon-echo. This term arises only in the presence of the local field. By varying the available parameters in the simulation, it rapidly becomes evident that while it is possible to reproduce the experimental results at negative delays for low and intermediate fields, it is not possible to do so for the data at positive delays and high fields where the behavior is dominated by polarization interference. In order to try and reproduce these results more fully, the simulation was modified to model two noninteracting two-level systems. This was achieved by eliminating all terms containing any link to the third level, (i.e., the second excited state) giving equations for a two-level system, and solving these for the two different transition energies. Figure 5 shows logarithmically the data from the two noninteracting two-level systems for the same parameters used for the three-level system in the data shown in Fig. 4. The signal at positive delays shows beats whose phase varies as a function of interpulse delay, (i.e., with gradient +1) corresponding to the well-known behavior expected for PI. At negative delay, the phase of the beats evolves in the same manner. This variation in the phase of the beats is typical of the behavior expected for two noninteracting two-level systems, where the beating is polarization interference.⁶ The other observed difference

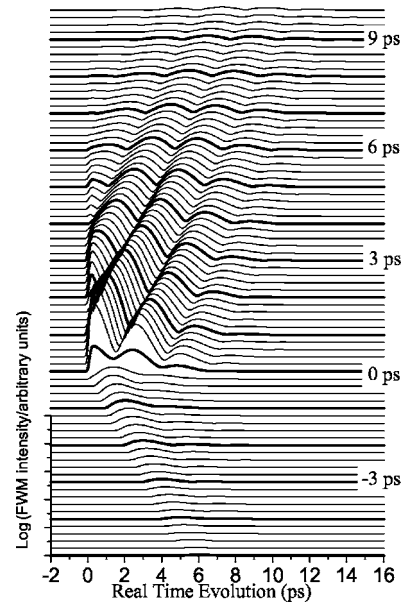


FIG. 5. Results for modeling two, noninteracting two-level systems, using the same parameters as for Fig. 4.

between this model and that for the three-level system, is the absence of beating as a function of τ .

Thus, this model is able to reproduce qualitatively the phase variation of the beats from the experimental results at positive delays for all magnetic fields, and the predominant behavior at high fields for all times. However, it does not predict the presence of beats as a function of τ , nor does it predict the observed variation of the phase of the beats at negative delays, for low and intermediate fields. Both models considered here predict the variation of the phase of the beats to be the same at negative delays as it is at positive delays. However, as can be seen in Figs. 2(a) and 2(b), this was clearly not the case for the experiments performed at low and intermediate magnetic fields.

At high fields, the experimental results can be modeled almost entirely by the two noninteracting two-level systems, as shown in Fig. 6, with the values for the coherence times increased to 5 ps, and inhomogeneous broadening reduced to 0.3 meV, consistent with the experimental observations. However, the experimental data still show the presence of beating as a function of τ , which is not reproduced by this model. In order to describe the experiments, one approach is to take a combination of the two models, which would represent contributions to the signal from two populations of exciton in the samples studied. The other major effect seen in the experiment, but not yet explained by either model, is the apparent π phase shift of the beats at negative delay. This occurs as a function of τ , at a frequency equal to the frequency of the beats in the real-time evolution, and can be reproduced by adding contributions from the two models. By adding the two components in the right ratio, the behavior of the beats can be reproduced well for all fields.

It is evident in the experimental data that as the magnetic field is increased, the system varies gradually from the case shown in Fig. 2(a) through to that shown in Fig. 2(b), and finally to the case shown in Fig. 2(c). From the results of the

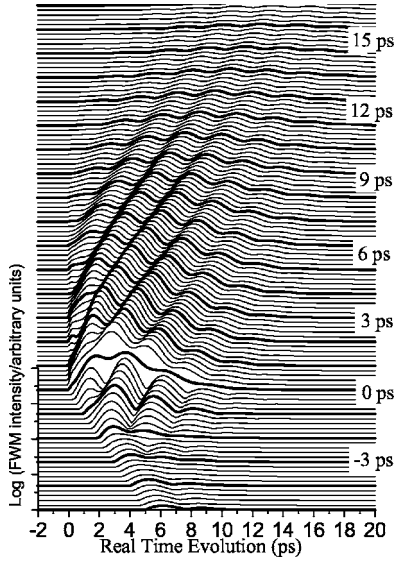


FIG. 6. Results plotted logarithmically for modeling two, non-interacting two-level systems, but with T_2 increased to 5 ps and inhomogeneous broadening reduced to 0.3 meV.

simulation, the change in behavior at negative delays can be attributed to an increase in the proportion of signal coming from noninteracting systems and a corresponding decrease in the amount from coupled systems. Meanwhile the increasing lifetimes and homogeneity are explained by the increasing confinement of the excitons generated by the magnetic field. Thus, we conclude that as the confinement is increased, the wave functions of excitons are reduced in size, and at some point, monolayer islands which were coupled, cease to be coupled. Due to the inhomogeneity in monolayer island size and shape, this occurs at different fields for different islands, and hence the transition is gradual as the field is increased. This suggests that whatever the coupling mechanism, it decreases in efficiency as the spatial extent of the exciton wave function is reduced.

Previous studies have suggested the dipole-dipole interaction as the source of coupling.⁵ However, if this were the case here, increasing the magnetic field would be expected to increase the dipole moment, which would lead to increased coupling. The opposite of this was observed, and so dipole-dipole interactions appear unlikely to explain the coupling mechanism in the sample studied here.

V. CONCLUSIONS

We have performed TR-FWM experiments on a GaAs/AlGaAs single quantum well and observed different behavior of the beats between excitons localized in monolayer islands as the applied magnetic field is changed. The sensitivity of our detection system allowed us to study the effects at negative pulse delays more closely than previously possible, with unexpected results. The four-wave-mixing emission shows evolution from free-polarization decay to photon echo as the time delay between the excitation pulses is increased. The evolution of the beat phase at positive delay indicates a predominant contribution from polarization inter-

ference, with a small contribution from genuine quantum beating manifesting itself as a modulation of the signals with delay. The gradient of the evolution of the beat phase with interpulse delay changes sign as the magnetic field is increased. Simulations of a coupled three-level system and two noninteracting two-level systems, with the inclusion of local field effects, were able to reproduce qualitatively all the major features of these results. The three-level system models the general case of coherently coupled excitons, and it was shown that as the magnetic field and thus the confinement increased, the contribution to the overall signal from this part of the model reduced. The possibility of the coherently coupled part of the signal being due to biexcitons as suggested by Finger *et al.*⁸ is ruled out as the excitation beams were cocircularly polarized. Thus we conclude that the coupling between monolayers is highly dependent on the extent of confinement and wave function overlap, and could be expected to vary significantly between different samples.

ACKNOWLEDGMENTS

V.B. thanks the CNRS institution for the sabbatical year spent in the Cavendish Laboratory. We are grateful to D. A. Ritchie for provision of a quantum well sample. This work was supported by the EPSRC.

APPENDIX

By following the different wave vector components that will give rise to the FWM signal in the $2k_2 - k_1$ direction through Eqs. (6)–(9), one obtains the following system of simultaneous first-order equations. Here we use the following notation: the wave vector component of each term is noted in the superscript as either (a) for k_1 or (b) for k_2 , so the electric field,

$$E = E_1 e^{i(k_1 \cdot r - \omega t)} + E_1 e^{-i(k_1 \cdot r - \omega t)} + E_2 e^{i(k_2 \cdot r - \omega t)} + E_2 e^{-i(k_2 \cdot r - \omega t)} \quad (\text{A1})$$

which in the rotating-wave approximation becomes

$$E = E_1 e^{i(k_1 \cdot r)} + E_2 e^{i(k_2 \cdot r)} \quad (\text{A2})$$

is represented as

$$E = E^{(a)} + E^{(b)} \quad (\text{A3})$$

The order of each of the density matrix and polarization terms is indicated by the corresponding number in the superscript. The zero-order terms correspond to no interaction and are thus the equilibrium values of the given terms. The terms of the form ω_j , where $j=2,3$ are equivalent to $\omega_{j1} = \omega_{jj} - \omega_{11} - \omega_0$. The first-order polarization terms are

$$P^{(1)(a)} = \mu_{12}^* \rho_{12}^{(1)(a)} + \mu_{13}^* \rho_{13}^{(1)(a)} + \mu_{12} \rho_{12}^{(1)(-a)*} + \mu_{13} \rho_{13}^{(1)(-a)*},$$

$$P^{(1)(-a)} = \mu_{12}^* \rho_{12}^{(1)(-a)} + \mu_{13}^* \rho_{13}^{(1)(-a)} + \mu_{12} \rho_{12}^{(1)(a)*} + \mu_{13} \rho_{13}^{(1)(a)*},$$

$$P^{(1)(b)} = \mu_{12}^* \rho_{12}^{(1)(b)} + \mu_{13}^* \rho_{13}^{(1)(b)} + \mu_{12} \rho_{12}^{(1)(-b)*} + \mu_{13} \rho_{13}^{(1)(-b)*},$$

$$P^{(1)(-b)} = \mu_{12}^* \rho_{12}^{(1)(-b)} + \mu_{13}^* \rho_{13}^{(1)(-b)} + \mu_{12} \rho_{12}^{(1)(b)*} + \mu_{13} \rho_{13}^{(1)(b)*}. \quad (\text{A4})$$

The relaxation terms are included as indicated in Eqs. (4) and (5)

So, the terms which contribute to the third-order polarization can be specified at each order as follows.

In the first order we have

$$\dot{\rho}_{12}^{(1)(a)} = \frac{i}{\hbar} \mu_{12}^* (E^{(a)} + LP^{(1)(a)}) [\rho_{22}^{(0)} - \rho_{11}^{(0)}] - \rho_{12}^{(1)(a)} \left(\frac{1}{T_{2(2)}} - i\omega_{21} \right) \quad (\text{A5})$$

$$\dot{\rho}_{12}^{(1)(b)} = \frac{i}{\hbar} \mu_{12}^* (E^{(b)} + LP^{(1)(b)}) [\rho_{22}^{(0)} - \rho_{11}^{(0)}] - \rho_{12}^{(1)(b)} \left(\frac{1}{T_{2(2)}} - i\omega_{21} \right) \quad (\text{A6})$$

$$\dot{\rho}_{12}^{(1)(-a)} = \frac{i}{\hbar} \mu_{12}^* LP^{(1)(-a)} [\rho_{22}^{(0)} - \rho_{11}^{(0)}] - \rho_{12}^{(1)(-a)} \left(\frac{1}{T_{2(2)}} - i\omega_{21} \right) \quad (\text{A7})$$

$$\dot{\rho}_{12}^{(1)(-b)} = \frac{i}{\hbar} \mu_{12}^* LP^{(1)(-b)} [\rho_{22}^{(0)} - \rho_{11}^{(0)}] - \rho_{12}^{(1)(-b)} \left(\frac{1}{T_{2(2)}} - i\omega_{21} \right) \quad (\text{A8})$$

$$\dot{\rho}_{13}^{(1)(a)} = \frac{i}{\hbar} \mu_{13}^* (E^{(a)} + LP^{(1)(a)}) [\rho_{33}^{(0)} - \rho_{11}^{(0)}] - \rho_{13}^{(1)(a)} \left(\frac{1}{T_{2(3)}} - i\omega_{31} \right) \quad (\text{A9})$$

$$\dot{\rho}_{13}^{(1)(b)} = \frac{i}{\hbar} \mu_{13}^* (E^{(b)} + LP^{(1)(b)}) [\rho_{33}^{(0)} - \rho_{11}^{(0)}] - \rho_{13}^{(1)(b)} \left(\frac{1}{T_{2(3)}} - i\omega_{31} \right) \quad (\text{A10})$$

$$\dot{\rho}_{13}^{(1)(-a)} = \frac{i}{\hbar} \mu_{13}^* LP^{(1)(-a)} [\rho_{33}^{(0)} - \rho_{11}^{(0)}] - \rho_{13}^{(1)(-a)} \left(\frac{1}{T_{2(3)}} - i\omega_{31} \right) \quad (\text{A11})$$

$$\dot{\rho}_{13}^{(1)(-b)} = \frac{i}{\hbar} \mu_{13}^* LP^{(1)(-b)} [\rho_{33}^{(0)} - \rho_{11}^{(0)}] - \rho_{13}^{(1)(-b)} \left(\frac{1}{T_{2(3)}} - i\omega_{31} \right). \quad (\text{A12})$$

In the second order

$$i\hbar \dot{\rho}_{22}^{(2)(b,b)} = + \mu_{12}^* \rho_{12}^{(1)(-b)*} (E^{(b)} + LP^{(1)(b)}) - \mu_{12} \rho_{12}^{(1)(b)} \times (LP^{(1)(-b)*}) - \frac{i\hbar}{T_{1(2)}} (\rho_{22}^{(2)(b,b)} - \rho_{22}^{(2eq)(b,b)}) \quad (\text{A13})$$

$$i\hbar \dot{\rho}_{33}^{(2)(b,b)} = + \mu_{13}^* \rho_{13}^{(1)(-b)*} (E^{(b)} + LP^{(1)(b)}) - \mu_{13} \rho_{13}^{(1)(b)} \times (LP^{(1)(-b)*}) - \frac{i\hbar}{T_{1(3)}} (\rho_{33}^{(2)(b,b)} - \rho_{33}^{(2eq)(b,b)}) \quad (\text{A14})$$

$$i\hbar \dot{\rho}_{22}^{(2)(-a,b)} = - \mu_{12} \rho_{12}^{(1)(b)} [E^{(a)*} + LP^{(a)*}] + \mu_{12}^* \rho_{12}^{(1)(-b)*} LP^{(-a)} + \mu_{12}^* \rho_{12}^{(1)(a)*} [E^{(b)} + LP^{(b)}] - \mu_{12} \rho_{12}^{(1)(-a)} LP^{(-b)*} - \frac{i\hbar}{T_{1(2)}} (\rho_{22}^{(2)(-a,b)} - \rho_{22}^{(2eq)(-a,b)}) \quad (\text{A15})$$

$$i\hbar \dot{\rho}_{33}^{(2)(-a,b)} = - \mu_{13} \rho_{13}^{(1)(b)} [E^{(a)*} + LP^{(a)*}] + \mu_{13}^* \rho_{13}^{(1)(-b)*} LP^{(-a)} + \mu_{13}^* \rho_{13}^{(1)(a)*} [E^{(b)} + LP^{(b)}] - \mu_{13} \rho_{13}^{(1)(-a)} LP^{(-b)*} - \frac{i\hbar}{T_{1(3)}} (\rho_{33}^{(2)(-a,b)} - \rho_{33}^{(2eq)(-a,b)}) \quad (\text{A16})$$

$$i\hbar \dot{\rho}_{23}^{(2)(b,b)} = + \mu_{13}^* \rho_{12}^{(1)(-b)*} [E^{(b)} + LP^{(1)(b)}] - \mu_{12} \rho_{13}^{(1)(b)} LP^{(1)(-b)*} - i\hbar \rho_{23}^{(2)(b,b)} \left(\frac{1}{T_{2(23)}} - i\omega_{32} \right) \quad (\text{A17})$$

$$i\hbar \dot{\rho}_{23}^{(2)(-b,-b)} = + \mu_{13}^* \rho_{12}^{(1)(b)*} LP^{(1)(-b)} - \mu_{12} \rho_{13}^{(1)(-b)} [E^{(1)(b)*} + LP^{(1)(b)*}] - i\hbar \rho_{23}^{(2)(-b,-b)} \left(\frac{1}{T_{2(23)}} - i\omega_{32} \right) \quad (\text{A18})$$

$$i\hbar \dot{\rho}_{23}^{(2)(a,-b)} = + \mu_{13}^* \rho_{12}^{(1)(b)*} [E^{(a)} + LP^{(1)(a)}] + \mu_{13}^* \rho_{12}^{(1)(-a)*} LP^{(1)(-b)} - \mu_{12} \rho_{13}^{(1)(a)} [E^{(b)*} + LP^{(1)(b)*}] - \mu_{12} \rho_{13}^{(1)(-b)} LP^{(1)(-a)*} - i\hbar \rho_{23}^{(2)(a,-b)} \left(\frac{1}{T_{2(23)}} - i\omega_{32} \right) \quad (\text{A19})$$

$$i\hbar \dot{\rho}_{23}^{(2)(-a,b)} = + \mu_{13}^* \rho_{12}^{(1)(a)*} [E^{(b)} + LP^{(1)(b)}] + \mu_{13}^* \rho_{12}^{(1)(-b)*} LP^{(1)(-a)} - \mu_{12} \rho_{13}^{(1)(b)} [E^{(a)*} + LP^{(1)(a)*}] - \mu_{12} \rho_{13}^{(1)(-a)} LP^{(1)(-b)*} - i\hbar \rho_{23}^{(2)(-a,b)} \left(\frac{1}{T_{2(23)}} - i\omega_{32} \right). \quad (\text{A20})$$

In the third order we have

$$i\hbar\dot{\rho}_{12}^{(3)(b,b,-a)} = [E^{(b)} + LP^{(1)(b)}] \times [-\mu_{12}^*(2\rho_{22}^{(2)(-a,b)} + \rho_{33}^{(2)(-a,b)}) - \mu_{13}^*\rho_{23}^{(2)(a,-b)*}] + [LP^{(1)(-a)}] \times [-\mu_{12}^*(2\rho_{22}^{(2)(b,b)} + \rho_{33}^{(2)(b,b)}) - \mu_{13}^*\rho_{23}^{(2)(-b,-b)*}] + LP^{(3)(b,b,-a)}\mu_{12}^* - i\hbar\rho_{12}^{(3)(b,b,-a)}\left(\frac{1}{T_{2(2)}} - i\omega_{21}\right) \quad (\text{A21})$$

$$i\hbar\dot{\rho}_{13}^{(3)(b,b,-a)} = [E^{(b)} + LP^{(1)(b)}] \times [-\mu_{13}^*(2\rho_{33}^{(2)(-a,b)} + \rho_{22}^{(2)(-a,b)}) - \mu_{12}^*\rho_{23}^{(2)(-a,b)}] + [LP^{(1)(-a)}] \times [-\mu_{13}^*(2\rho_{33}^{(2)(b,b)} + \rho_{22}^{(2)(b,b)}) - \mu_{12}^*\rho_{23}^{(2)(b,b)}] + LP^{(3)(b,b,-a)}\mu_{13}^* - i\hbar\rho_{13}^{(3)(b,b,-a)}\left(\frac{1}{T_{2(3)}} - i\omega_{31}\right). \quad (\text{A22})$$

-
- ¹M. Hoffmann, S. D. Brorson, J. Mork, and A. Mecozzi, *Appl. Phys. Lett.* **68**, 3236 (1996).
²A. Mecozzi and J. Mork, *J. Opt. Soc. Am. B* **13**, 2437 (1996).
³P. Borri, W. Langbein, S. Schneider, U. Woggon, R. L. Sellin, D. Ouyang, and D. Bimberg, *Phys. Rev. Lett.* **87**, 157401 (2001).
⁴P. Borri, W. Langbein, J. Mork, J. M. Hvam, F. Heinrichsdorff, M. H. Mao, and D. Bimberg, *Phys. Rev. B* **60**, 7784 (1999).
⁵M. Koch, J. Feldmann, E. O. Gobel, P. Thomas, J. Shah, and K. Kohler, *Phys. Rev. B* **48**, 11480 (1993).
⁶M. Koch, J. Feldmann, G. von Plessen, E. O. Gobel, P. Thomas, and K. Kohler, *Phys. Rev. Lett.* **69**, 3631 (1992).
⁷A. Euteneuer, E. Finger, M. Hofmann, W. Stolz, T. Meier, P. Thomas, S. W. Koch, W. W. Ruhle, R. Hey, and K. Ploog, *Phys. Rev. Lett.* **83**, 2073 (1999).
⁸E. Finger, S. Kraft, A. Euteneuer, M. Hofmann, W. Stolz, and W. W. Ruhle, *Phys. Status Solidi B* **221**, 373 (2000).
⁹D. J. Lovering, R. T. Phillips, G. J. Denton, and G. W. Smith, *Phys. Rev. Lett.* **68**, 1880 (1992).
¹⁰D. Birkedal, V. G. Lyssenko, K.-H. Pantke, J. Erland, and J. M. Hvam, *Phys. Rev. B* **51**, 7977 (1995).
¹¹X. J. Zhu, M. S. Hybertsen, P. B. Littlewood, and M. C. Nuss, *Phys. Rev. B* **50**, 11915 (1994).
¹²J. M. Hvam, V. G. Lyssenko, and D. Birkedal, *Pure Appl. Chem.* **67**, 401 (1995).
¹³Arthur L. Smirl, Martin J. Stevens, X. Chen, and O. Buccafusca, *Phys. Rev. B* **60**, 8267 (1999).
¹⁴Hailin Wang, Kyle Ferrio, Duncan G. Steel, Y. Z. Hu, R. Binder, and S. W. Koch, *Phys. Rev. Lett.* **71**, 1261 (1993).
¹⁵N. H. Kwong, I. Rumyantsev, R. Binder, and Arthur L. Smirl, *Phys. Rev. B* **72**, 235312 (2005).
¹⁶O. Carmel and I. Bar-Joseph, *Phys. Rev. B* **47**, 7606 (1992).
¹⁷M. Wegener, D. S. Chemla, S. Schmitt-Rink, and W. Schafer, *Phys. Rev. A* **42**, 5675 (1990).
¹⁸K. Leo, M. Wegener, J. Shah, D. S. Chemla, E. O. Gobel, T. C. Damen, S. Schmitt-Rink, and W. Schafer, *Phys. Rev. Lett.* **65**, 1340 (1990).
¹⁹A. Honold, L. Schultheis, J. Kuhl, and C. W. Tsu, *Appl. Phys. Lett.* **52**, 2105 (1988).
²⁰D. Gammon, E. S. Snow, B. V. Shanabrook, D. S. Katzer, and D. Park, *Phys. Rev. Lett.* **76**, 3005 (1996).
²¹M. D. Webb, S. T. Cundiff, and D. G. Steel, *Phys. Rev. Lett.* **66**, 934 (1991).
²²M. Hubner, J. Kuhl, B. Grote, T. Stroucken, S. W. Koch, R. Hey, and K. Ploog, *Solid State Commun.* **108**, 787 (1998).
²³S. T. Cundiff, *Phys. Rev. A* **49**, 3114 (1994).
²⁴T. Yajima and Y. Taira, *J. Phys. Soc. Jpn.* **47**, 1620 (1979).
²⁵M. Koch, J. Feldmann, G. von Plessen, S. T. Cundiff, E. O. Gobel, P. Thomas, and K. Kohler, *Phys. Rev. Lett.* **73**, 210 (1994).